Climatic Change (2010) 98:331–357
DOI 10.1007/s10584-009-9736-6

# CMIP3 projected changes in the annual cycle of the South American Monsoon

**Anji Seth · Maisa Rojas · Sara A. Rauscher**

Received: 23 June 2008 / Accepted: 3 August 2009 / Published online: 17 October 2009


**Abstract** Nine models from the Coupled Model Intercomparison Project version 3 dataset are employed to examine projected changes in the South American Monsoon System annual cycle by comparing the 20th Century and SRES A2 scenarios. The following hypotheses are examined: (1) the warm season climate responses in the Southeast, Continental South Atlantic Convergence Zone (CSACZ) and Monsoon regions are related by regional circulation and moisture transport changes which, in turn, must be consistent with robust large-scale changes in the climate system, and (2) an increased threshold for convection in a warmer world may affect the timing of warm season rains. The present analysis reaffirms that the Southeast region is likely to experience increased precipitation through the warm season. Additional results exhibit more uncertainty due to large inter-model variance and disagreement in the A2 scenarios. Nevertheless several statistically significant results are found. In the Monsoon and to a lesser extent in the CSACZ region, the multi-model median suggests reduced precipitation during spring (Sep–Nov). These continental precipitation changes are accompanied by a southward shift of the maximum precipitation in the South Atlantic Convergence Zone. Changes in circulation include a poleward displaced South Atlantic Anticyclone (SAAC) and enhanced moisture transport associated with a strengthened northerly low level flow east of the Andes during spring. Moisture transport divergence calculations indicate unchanged divergence in the Monsoon region during spring and increased convergence in the Southeast

A. Seth (✉)
Department of Geography, University of Connecticut,
215 Glenbrook Road, Unit 4148, Storrs, CT 06269-4148, USA
e-mail: anji.seth@uconn.edu

M. Rojas
Universidad de Chile, Santiago, Chile

S. A. Rauscher
Earth System Physics Section, The Abdus Salam International Centre
for Theoretical Physics, Trieste, Italy

throughout the warm season. The circulation and moisture transport changes suggest the increased precipitation in the Southeast during spring may be related to changes in the SALLJ and SAAC, which both enhance moisture transport to the Southeast. The seasonally dry Monsoon region is further affected by an increased threshold for convection in the warmer, more humid and stable climate of the 21st century, which combined with the circulation changes may weaken the onset of the rainy season. Although there is substantial variability among the models, and the results are represented by small changes compared with the multi-model variance, the statistical significance and consistency with expected robust large scale changes provide a measure of confidence in otherwise tentative results. Further testing of the relationships presented here will be required to fully understand projected changes in the South American Monsoon.

## 1 Introduction

Analysis of continental and regional scale responses to anthropogenic forcing of greenhouse gases is currently underway using the Coupled Model Intercomparison Project version 3 (CMIP3) datasets e.g., Meehl et al. (2007), which were employed by the Intergovernmental Panel on Climate Change (IPCC) in the Fourth Assessment Report (AR4) (Solomon and Qin 2007). The South American climate response has been recently examined at the continental scale (Vera et al. 2006c) as well as for the Amazon basin (Li et al. 2006). Li et al. (2006) emphasize a substantial disagreement among the subset of models studied on the direction of change in summer precipitation in the Amazon Basin. Even models that perform well in the 20th century disagree on future changes, and detailed analysis of two models suggests the coupled model SST response is a major factor in the disagreement. In contrast to the disparate results for the Amazon, Vera et al. (2006c) show agreement among a subset of models in projecting increased summer precipitation over southeastern subtropical South America (SESA, see Fig. 1). The results in this region are consistent with observations, which have shown an increasing trend in precipitation during the latter half of the 20th century (Liebmann et al. 2004).

In this research the CMIP3 dataset is further exploited to examine changes in the South American Monsoon System (SAMS) annual cycle, with emphasis on the SESA and the core and extended Monsoon regions which comprise important population and economic centers for the continent. With a goal toward improved understanding of the regional projections, this analysis examines multi-model ensemble statistics related to circulation, moisture transport, and surface latent heat flux changes, which describe potential outcomes while highlighting the uncertainties. Our purpose is to discuss mechanisms associated with projected changes in precipitation and temperature within the context of global circulation changes which have previously been shown to be robust.

The present-day climate of subtropical South America experiences a distinct annual cycle in rainfall associated with the SAMS, with most rainfall occurring during the austral summer (Zhou and Lau 1998; Vera et al. 2006b); the SESA region also receives cold season precipitation from mid-latitude frontal systems (Vera et al. 2006b). A major feature of the SAMS is the South Atlantic Convergence Zone (SACZ), a region of enhanced convection that extends diagonally across central South America

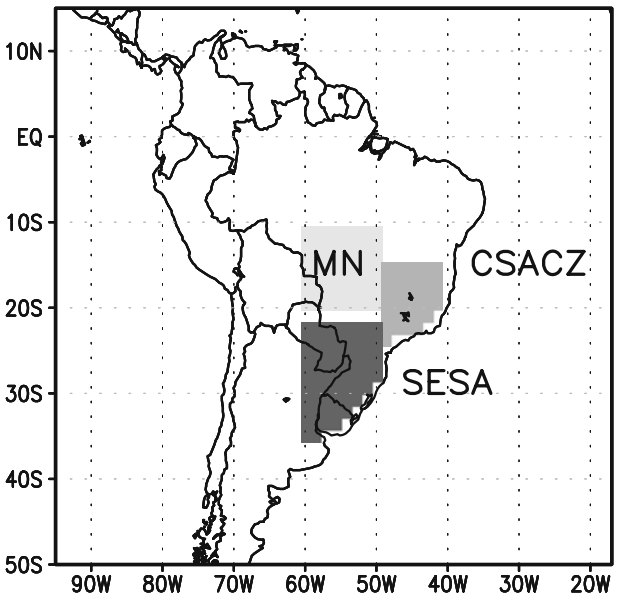


**Fig. 1** Regions of analysis in this study: Monsoon (50–60W, 10–20S), Continental SACZ (*CSACZ*: 40–50°W, 15–25°S) and Southeastern South America (*SESA*: 50–60°W, 22–35°S)

from the northwest to the southeast into the South Atlantic Ocean (Kodama 1992, 1993; Carvalho et al. 2004). The moisture sources for warm season precipitation are the tropical Atlantic and the Amazon basin.

There are two main pathways of moisture transport from the Amazon into the subtropics (Nogués-Paegle and Mo 1997; Herdies et al. 2002): (1) a low-level northerly flow located east of the Andes Mountains which is diurnally forced, can be seen in reanalysis products, and is referred to as the South American Low Level Jet (SALLJ) (Nogués-Paegle and Mo 1997) and (2) a northerly flow from the continent into the SACZ that occurs to the east of the SALLJ and on the western flank of the South Atlantic anticyclone (SAAC) (Herdies et al. 2002). These two moisture transport pathways are associated with a dipole mode of variability wherein enhanced precipitation in the SACZ is accompanied by reduced rainfall in the subtropical plains of SESA (Nogués-Paegle and Mo 1997). The opposite phase is associated with increased southward moisture transport from the Amazon basin and more precipitation in SESA (Diaz and Aceituno 2003). As part of this dipole structure, low-level westerly (easterly) winds are observed during active (inactive) SACZ with net divergence (convergence) over the SESA, eastward (westward) displacement of the SAAC, and a weak (strong) SALLJ (Herdies et al. 2002; Vera et al. 2006b). It must be noted that the SALLJ includes observed diurnally varying mesoscale features (Virji 1981; Paegle 1998; Berbery and Barros 2002; Marengo et al. 2002, 2004; Vera et al. 2006a) which are not represented in the coarse scale reanalysis and climate models. Since the analysis presented here employs monthly mean atmospheric fields, which cannot describe episodic jet events, our use of SALLJ refers simply to the mean low level northerly flow in the reanalysis and climate models.

There is evidence linking SACZ variability to ENSO (Carvalho et al. 2004). In addition, intensification of the SALLJ is associated with warm ENSO events (Berbery

and Barros 2002). However, the observed increasing trend in precipitation in SESA appears to be correlated with higher SSTs and weaker winds in the western circulation of the SAAC in the nearby subtropical South Atlantic Ocean (Liebmann et al. 2004), and has yet to be linked to the large-scale warm ENSO-like changes associated with greenhouse warming. Finally, evaluation of the CMIP3 models for the present day climate shows that while the models adequately represent warm season continental precipitation associated with the SAMS, they do not simulate its oceanic extension into the SACZ well (Vera et al. 2006c).

Analysis of the CMIP3 dataset for the 21st century indicates an overall weakening of the tropical circulation. This weakening is seen dominantly in the Walker circulation (Vecchi and Soden 2007; Held and Soden 2006): the large-scale convective overturning must slow to compensate for the fact that atmospheric water vapor increases more than precipitation in a warmer world. Vecchi and Soden (2007) map the change in vertical velocity per degree of global warming in their Figure 7b, which shows enhanced upward motion in the eastern tropical Pacific and reduced upward motion in the western tropical Pacific. This mean atmospheric response is similar to the warm phase of ENSO, and consistent with this result, over the South American continent enhanced subsidence is seen over the Amazon basin and enhanced vertical motion in SESA. In addition, the increased subsidence in the Amazon extends into the SACZ region, which appears to be associated with a poleward shift in the SAAC. Enhanced subsidence poleward and reduced subsidence equatorward of present day oceanic sub-tropical anticyclones indicates their poleward strengthening and shift. These results are also consistent with the "upped ante" mechanism (Neelin et al. 2003; Lintner and Neelin 2006); because a warmer, more humid atmosphere is more stable, it requires more moist static energy to initiate convection. Subtropical regions along the margins of precipitation, such as the seasonally dry Monsoon region, are especially disadvantaged according to this "upped ante" mechanism.

It is proposed that these robust large-scale dynamical responses can inform the regional results from Vera et al. (2006c) and Li et al. (2006) in the following ways. First, in the CMIP3 21st century projections, a warm ENSO-like atmospheric response suggests that consistent changes over the South American continent include subsidence in the Amazon and the increased precipitation over SESA, see Fig. 7 in Vecchi and Soden (2007). This result is indeed consistent with the present day observed relationship between ENSO and South American climate (Kousky et al. 1984; Ropelewski and Halpert 1987; Marengo 1992). Second, an increased moist static energy threshold for convection may affect the timing of the warm season rains. In working toward improved understanding of the CMIP3 regional projections for South America, this analysis explores the Monsoon, continental SACZ (hereafter, CSACZ) and SESA regions' annual cycles of temperature and precipitation, with an emphasis on the mechanisms underlying changes in 21st century temperature and precipitation.

The remainder of this paper is structured as follows. Section 2 describes the CMIP3 datasets and observations, as well as the analysis methods, including statistical representations of uncertainty, which are employed for the Monsoon, CSACZ and SESA regions (Fig. 1). Section 3 presents the results, beginning with a discussion of coupled climate model ensemble precipitation and temperature statistics compared with observed estimates. Twenty-first century projections are then discussed and followed by analysis of simulated and projected circulation (SACZ, SAAC,

SALLJ) and moisture transport. Section 4 presents discussion of the mechanisms underlying the projected changes and conclusions.

## 2 Methods and data

Model simulations from nine coupled climate models in the CMIP3 database are analyzed. Each of the selected models is well established and has a substantial record of published results (see Table 1, more information about the models can be found at http://www-pcmdi.llnl.gov/ipcc/model_documentation/ipcc_model_documentation.php and Meehl et al. 2007). Climate of the 20 Century experiments (hereafter, 20C) and the IPCC Special Report on Emission Scenarios (SRES) A2 scenario (hereafter, A2) for future climate change were examined. The A2 scenario describes a world of medium economic growth, but high population growth and energy use with slow economic and technological development. This leads to CO2 concentrations increasing rapidly, reaching 850 ppm by the year 2100. Previous work has shown that the patterns of regional precipitation change are relatively insensitive to the scenario (Giorgi and Bi 2005). Indeed, the future changes in precipitation noted in the SRES A1B simulations by Vera et al. (2006b) are consistent with the A2 results presented here.

Model ensemble statistics for the period 1971–2000 are compared with observed estimates of monthly mean values for temperature, precipitation, sea level pressure, moisture flux divergence and surface latent heat flux. Analysis of future climate is performed by computing the difference between the 2071–2100 and 1971–2000 periods. The ensemble coupled climate model statistics are represented using box plots which show monthly values of median, upper and lower quartiles and outliers). The median illustrates the central value and is less influenced by outliers than the arithmetic mean. These statistics are similar to the those employed by Kharin et al. (2007) and are described in detail in Wilks (2005). Although the ensemble of models cannot span all possible climate system responses (Allen et al. 2000), the plots show the spread in the model behavior, which can be used as a coarse measure of uncertainty. In addition, significance tests (student t) have been performed on the A2-20C differences between the means assuming unequal variances and $\alpha = 0.1$.

The focus of the analysis is on three regions in South America: the core Monsoon region [50–60°W, 10–20°S] (Gan et al. 2004, 2006), the southeast extension

**Table 1** CMIP3 coupled ocean-atmosphere models employed in this analysis

| Model name | Sponsor | Atm res. lat × lon | Ocean res. lat × lon |
|---|---|---|---|
| CCSM3, 2005 | NCAR | 1.4 × 1.4 | .3–1 × 1 |
| PCM, 1998 | NCAR | 2.8 × 2.8 | 0.5–0.7 × 1.1 |
| ECHAM5/MPI-OM, 2005 | Max Planck Institute | 1.9 × 1.9 | 1.5 × 1.5 |
| HadCM3, 1997 | Hadley Centre | 2.5 × 3.75 | 1.25 × 1.25 |
| GFDL CM2.1, 2005 | GFDL | 2.0 × 2.5 | 0.3–1 × 1 |
| IPSL CM4, 2005 | IPSL | 2.5 × 3.75 | 2 × 2 |
| HadGEM1, 2004 | HadGEM1 | 1.3 × 1.9 | 0.3–1 × 1 |
| MIROC3.2, 2004 | JAMSTEC | 2.8 × 2.8 | 0.5–1.4 × 1.4 |
| CSIRO Mk3, 2001 | CSIRO | 1.9 × 1.9 | 0.8 × 1.9 |

of the monsoon or continental SACZ region [40–50°W, 15–25°S] (hereafter, CSACZ) (Carvalho et al. 2004), and Southeastern South America (SESA) [50–60°W, 23–35°S] (Carvalho et al. 2002; Liebmann et al. 2004), all of which are shown in Fig. 1. The 20C simulated precipitation is evaluated using the Climate Prediction Center Merged Analysis of Precipitation (CMAP) (Xie and Arkin 1996), which is a blended product of global satellite and gauge data on a 2.5° latitude-longitude grid with monthly time resolution. Simulated surface air temperature, atmospheric circulation and moisture variables are compared against estimates from the NCEP/NCAR Reanalysis Project (NNRP) (Kalnay et al. 1996). Reanalysis data are employed for the analysis of vertically integrated moisture transport using monthly mean fields of horizontal winds (u,v) and specific humidity (q).

## 3 Results

The simulated 20C ensemble statistics are compared with observed estimates before examining projections of temperature and precipitation from the A2 scenario. These results are followed by analysis of changes in 21st century circulation and moisture transport variables projected in the A2 scenario simulations. In the results presented, area-averaged quantities employ the boundaries for the Monsoon, CSACZ and SESA regions given in Fig. 1.

### 3.1 Model verification

We begin with an ensemble mean view of precipitation for the early rainy season (Sep–Nov, SON) and the main rainy season (Dec–Feb, DJF). The observed estimates from CMAP (top) and ensemble mean 20C precipitation computed from the coupled models (middle) are shown in Fig. 2. During the early rainy season the ensemble mean captures the southeast extension of rainfall, although the simulated Atlantic ITCZ is weaker than the observed amplitude and appears to be shifted southward of the equator. In DJF the fully formed monsoon is well captured in all three continental regions (Monsoon, CSACZ and SESA) despite a lack of extension of the SACZ into the subtropical Atlantic and problems with the ITCZ in both ocean basins. There is also an overestimation of precipitation over the Andes which is not seen in the observed estimate. Still, the mean simulated precipitation patterns from the models appear to adequately represent observations for this analysis.

Figure 3a, b, c shows the climatological annual cycles of area-averaged precipitation from the 20C simulations (box plots) and NNRP (black) for the three analyzed regions. The box plots represent the monthly values of median (red) and interquartile range (blue). Whiskers represent 1.5 times the interquartile range and plus symbols (red) depict outlier values. In the Monsoon region, the models capture the large annual cycle, but the model median shows a delay in both the onset and demise of rainfall by approximately one month. In the CSACZ region precipitation is underestimated during the dry season and weaker than observed during SON. In SESA, the models simulate warm season rains well, but underestimate winter precipitation which is associated with frontal passages (Vera et al. 2006b). In all three

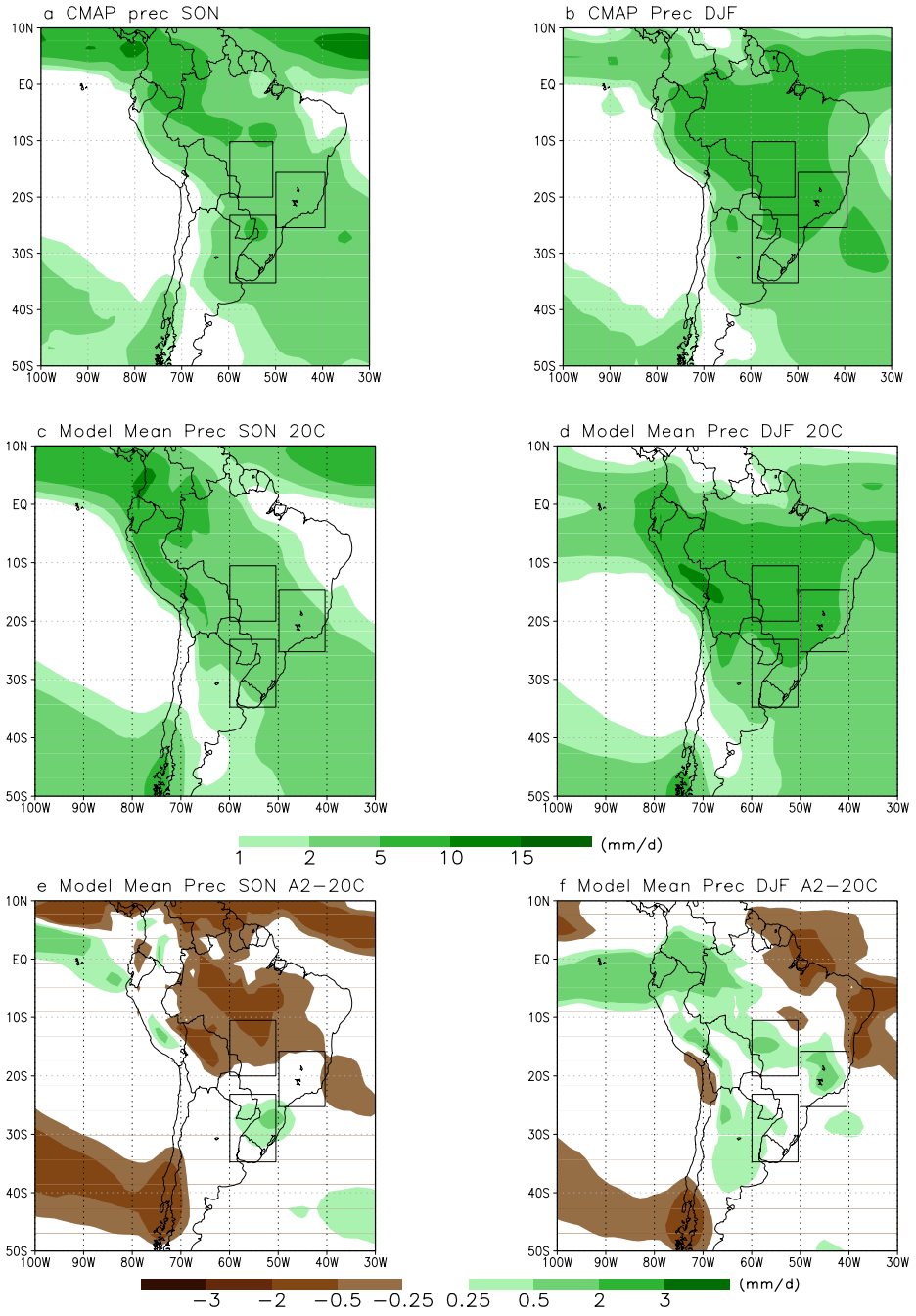


**Fig. 2** Seasonal mean precipitation (mm/day) SON (*left*) and DJF (*right*) for CMAP (**a**, **b**), and for multi-model mean 20C (**c**, **d**), and difference A2-20C (**e**, **f**)

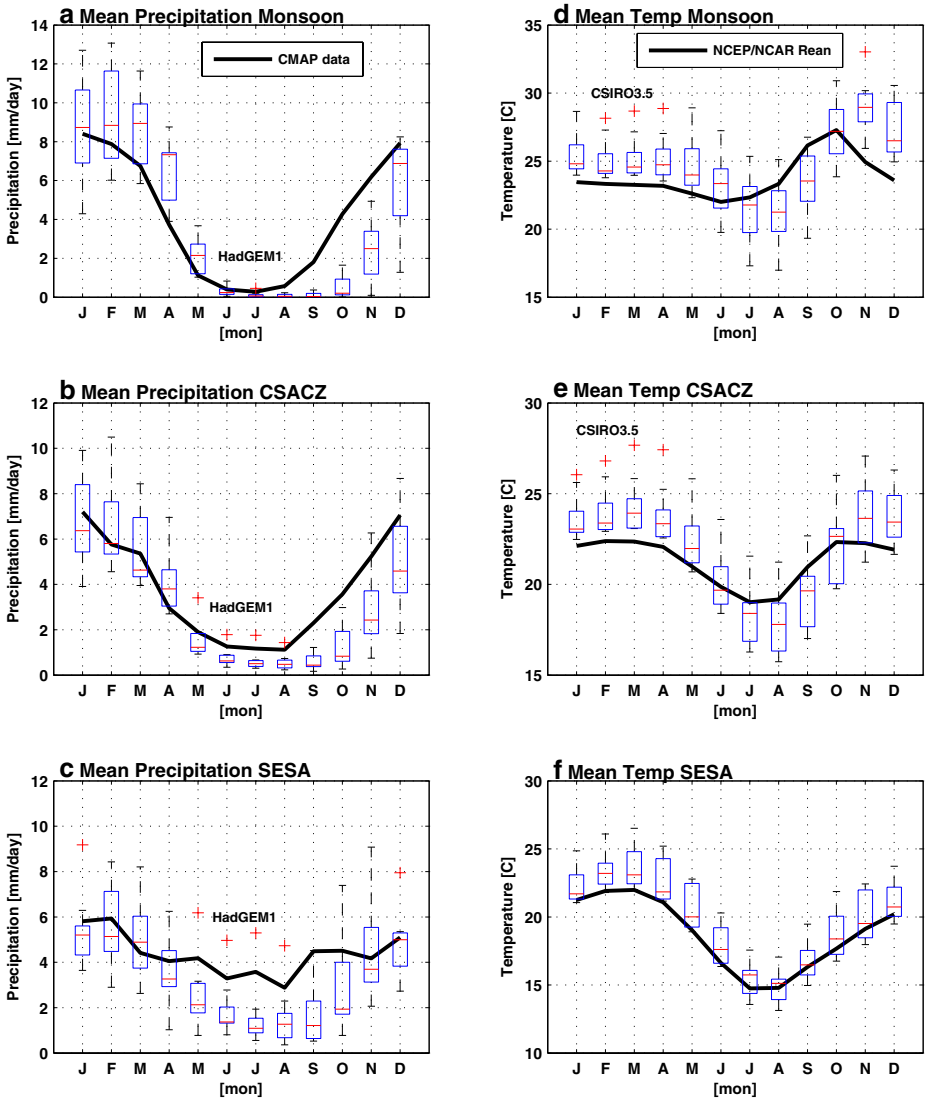


**Fig. 3** 20C monthly mean observed and simulated precipitation statistics in **a** Monsoon, **b** CSACZ and **c** SESA regions, and surface air temperature (**d**, **e**, **f**), with multi-model median (*red*), inter-quartile range (*blue*) and outlier (*red plus*) statistics shown as *boxplots*. Observed estimates (*black*) for precipitation are from CMAP and for temperature are from NNRP

regions the inter model variability is larger during the rainy season, while outlier values from the HadGEM1 occur primarily during the cold season.

The simulated and observed annual cycles of surface air temperature are given in Fig. 3d, e, f. The Monsoon region exhibits a relatively small annual cycle, with fairly constant temperatures around a mean of 24°C and a maximum in September of about 26°C. The models capture reduced temperatures during winter, and the highest temperatures which occur in spring, but amplify the amplitude of the annual

cycle (colder winter, warmer spring), and both minimum and maximum lag a month behind the observations. The models also show a small warm bias during the rainy season. In the CSACZ region the models do show a larger amplitude in the annual cycle than in the Monsoon region, similar to observations, but again the amplitude is larger and lags by a month the observations. SESA exhibits the largest annual cycle in temperature, which is captured by the median of the models in both phase and amplitude, except for a small warm bias during the late warm season. Extreme warm value outliers occur in the CSIRO3.5 model during the rainy season in the Monsoon and SACZ regions. The SESA region exhibits no outliers in temperature and smaller inter-quartile range, especially in winter when dynamical influences dominate over sub-grid scale physics in determining the temperature field.

In summary. the multi-model ensemble statistics are able to represent the main features related to the observed annual cycle of precipitation and temperature. Biases include a lag in simulated precipitation and underestimation of winter precipitation in SESA, and a warm bias during summer.

### 3.2 21st century projections

The multi-model ensemble precipitation differences (A2-20C) are shown in Fig. 4a, b, c which demonstrates changes in the median, and Table 2 presents the difference between the means with those significant at the 90% level of confidence in bold text. In the Monsoon region, the models hint at a small increase in precipitation during the late rainy season (Feb–Apr), as the median model response is above the zero line, but there is clear disagreement among the models, with MIROC3.2 as a negative outlier and ECHAM5 a positive outlier. During the dry season (May–Aug) changes are projected to be very small and the models are in agreement. The mean changes (Table 2) are small and negative, but significant. In the SAMS onset period (SON), the model statistics indicate a possible decrease in precipitation and the mean differences (Table 2) are larger and negative, and significant during the early rainy season (SON). For example, there is a significant 15% decrease in precipitation projection for the Monsoon region in October. Changes in the CSACZ region are in many ways similar to those seen in the Monsoon region: a small potential increase during the later rainy season (Feb–Mar) and a small drying during the early rainy season. In this region too, the early season drying is significant (Sep: −14%, Oct: −8%, Nov: −5% from Table 2). In contrast, changes in SESA precipitation indicate increases during much of the year, with the largest increases during the warm season rains (Oct–Feb); significant increases are found in the mean during the first half of the season (Oct: 11%, Nov: 17%, Dec: 9%, Jan: 6%).

Figure 4d, e, f show the difference in surface air temperature between the A2 and 20C simulations for our three regions. All models simulate warming for the A2 scenario and the differences between the means are statistically significant for every month in all three regions (not shown). In the Monsoon region the model median warming ranges from 3–5°C, with the largest increases during spring (OND) and smallest during the late rainy season (Feb–Apr). The CSACZ region is moderated by its coastal location and shows slightly smaller temperature changes as well as inter-model variability, with negative outliers from the NCAR/PCM1. Here too the largest median change is in Nov and smallest in Feb. In SESA the largest median increases in temperature occur during the winter months (May–Jul), notably when there is

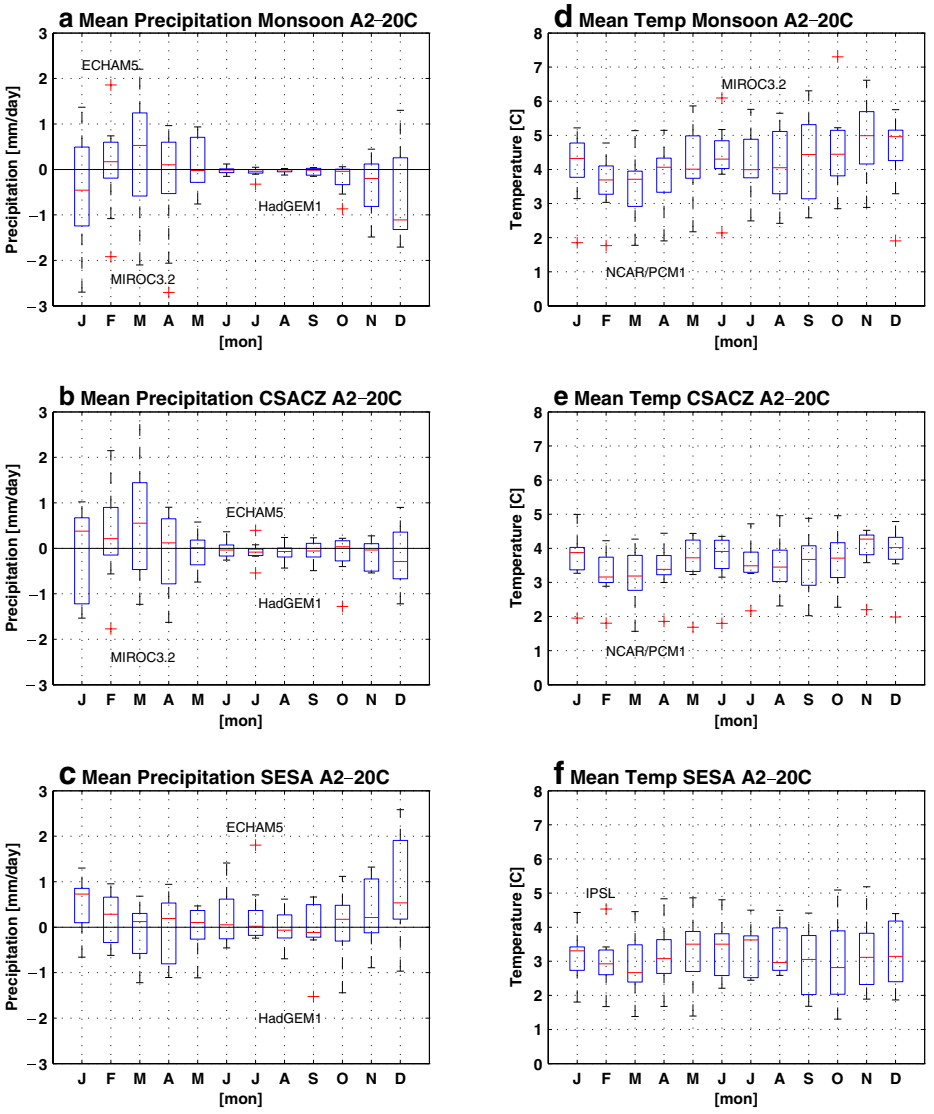


**Fig. 4** Multi-model ensemble statistics for monthly mean differences, A2-20C, in precipitation for **a** Monsoon, **b** CSACZ and **c** SESA regions and similarly for surface temperature (**c**, **d**, **e**), with multi-model median (*red*), inter-quartile range (*blue*) and outlier (*red plus*) statistics shown as *boxplots*

little projected change in precipitation. The larger median temperature increases in the Monsoon and CSACZ regions in spring are consistent with decreases in early season precipitation (Fig. 4a, b), and suggests a possible weakening of rains during the onset period. In contrast, SESA shows an increase in median precipitation during the onset period and through January, while little change is projected during the rest of the year. Thus, in all regions a larger amplitude is projected in the median annual cycle, due to increased precipitation during peak rains. However, the Monsoon and

**Table 2** Mean difference (A2-20C) in monthly precipitation (mm day, top) and percent difference (%, bottom)

| Month | Jan | Feb | Mar | Apr | May | Jun | Jul | Aug | Sep | Oct | Nov | Dec |
|---|---|---|---|---|---|---|---|---|---|---|---|---|
| MONSOON | 0.15 | 0.37 | −0.14 | 0.06 | −0.04 | **−0.06** | **−0.04** | **−0.05** | **−0.23** | **−0.38** | **−0.47** | −0.27 |
| CSACZ | 0.29 | **0.50** | −0.06 | −0.06 | −0.06 | **−0.12** | **−0.11** | **−0.11** | **−0.16** | **−0.20** | **−0.26** | −0.23 |
| SESA | **0.25** | −0.08 | −0.02 | −0.03 | 0.12 | **0.22** | −0.02 | 0.00 | 0.05 | **0.38** | **0.63** | **0.35** |
| MONSOON | 1.63 | 4.34 | −2.25 | 3.54 | −13.96 | **−46.96** | **−44.68** | **−38.00** | **−37.05** | **−14.95** | **−7.97** | −3.05 |
| CSACZ | 4.58 | **9.49** | −1.64 | −3.72 | −6.86 | **−17.20** | **−17.78** | **−17.26** | **−14.16** | **−7.51** | **−5.49** | −3.55 |
| SESA | **6.06** | −1.98 | −0.48 | −1.19 | 4.92 | **10.90** | −1.24 | −0.24 | 1.91 | **10.83** | **17.10** | **8.80** |

CSACZ regions suggest the possibility of a drier onset period while SESA exhibits enhanced rainfall during this period.

This drier onset period in the Monsoon region can be seen in Fig. 5c, which shows standardized precipitation differences (A2-20C, shading) and the multi-model

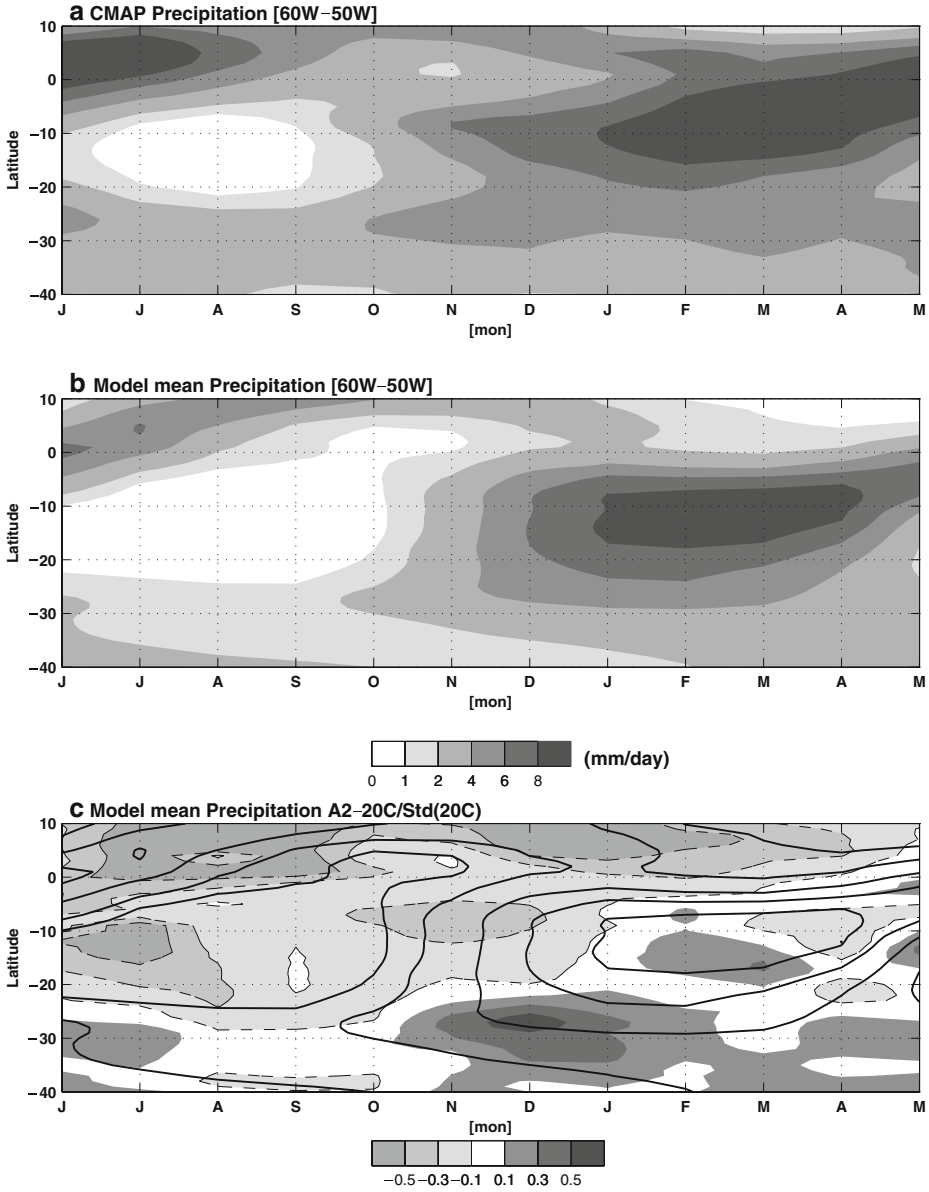


**Fig. 5** Time-latitude monthly mean precipitation (mm/day) averaged for 50°–60°W **a** 1979–1999 CMAP, **b** 20C multi-model mean and **c** difference A2-20C standardized by 20C (*shaded*), with multi-model climatological precipitation (*black lines*)

mean climatology (lines, also 5b shading) averaged from 50°W–60°W and viewed in latitude versus month coordinates. The dry season intensifies and the drying extends into the early rainy season (Oct–Dec) between 10°S–20°S. Once the rains are established the peak rainy season is wetter. This implies a shift toward later and more intense warm season rains in the Monsoon region. Between 20°–30°S, the models indicate an increase in precipitation through most of the warm season, especially in Nov–Jan, which is consistent with the observed trends in SESA. The upper panels of Fig. 5 show the present day latitude-time annual cycle of precipitation from CMAP and the multi-model mean. The models simulated well the warm season rains, though onset is later in the models by one month. The subtropical/midlatitude

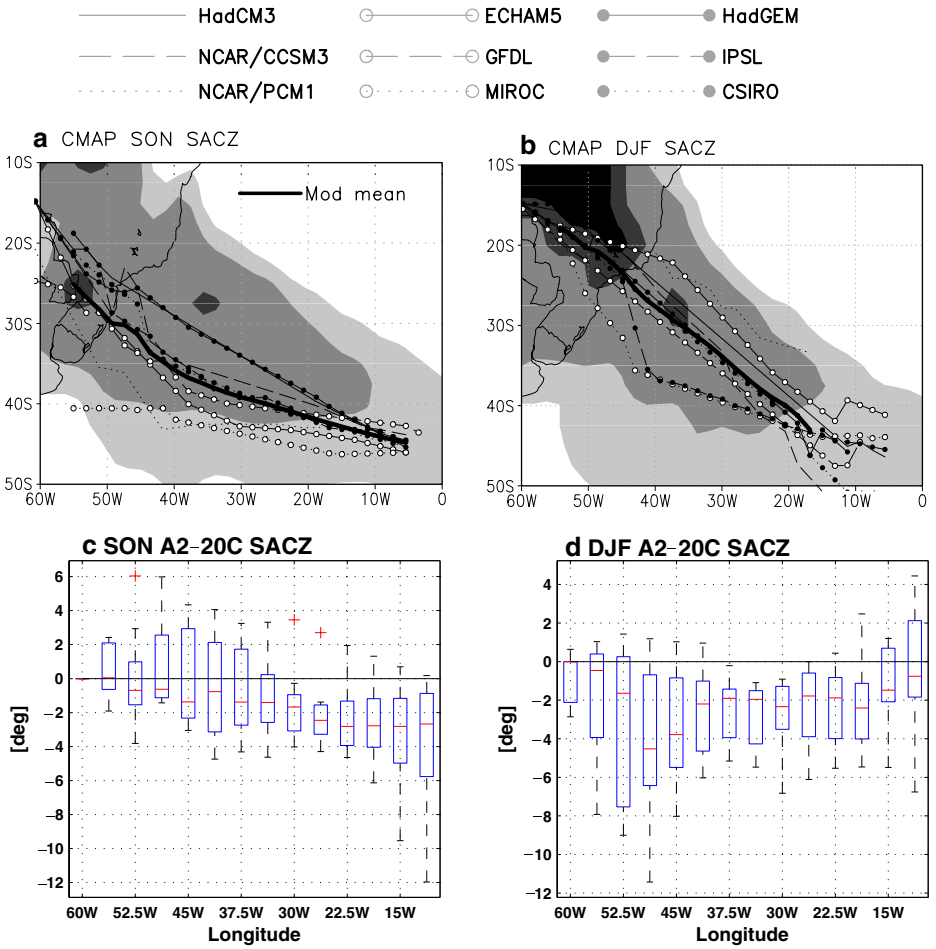


**Fig. 6** Simulated latitude of maximum precipitation as proxy of South Atlantic Convergence Zone: **a** 20C SON, **b** 20C DJF with model mean (*solid black*) and precipitation (*shaded*). A2-20C ensemble statistics for **c** SON and **d** DJF

frontal precipitation is also generally weak during winter compared with the CMAP estimates and seen also by Vera et al. (2006c).

During spring (Sep–Nov) and summer (Dec–Feb), the Monsoon precipitation over the continent extends into the Atlantic ocean forming the SACZ. Figure 6 shows the simulation of the SACZ by plotting the latitude of maximum precipitation against longitude for SON 20C (a), and DJF 20C (b) and A2 minus 20C (bottom panels). In spring, the models place the SACZ too far south. Although the models do not correctly simulate the amount of precipitation over the subtropical Atlantic (as shown in Fig. 2), the position of the SACZ in DJF is well-simulated. The model ensemble statistics suggest a southward shift of the SACZ during both spring and summer in the A2 simulations compared to the 20C simulations. Statistical significance tests on the difference between the mean latitude show the results are significant above the 90% level at all longitudes (not shown). Vera et al. (2006b) diagnosed increased precipitation in the SESA region in the CMIP3 models; here this increase is confirmed with an added potential of a southward shift of the region of maximum precipitation in the SACZ. This southward shift might be associated with a more prevalent inactive phase of the SACZ dipole in the future or a southward shift of the SAMS and the SACZ. These ideas are further explored by examining circulation changes.

## 3.3 Circulation changes

In order to explain the projected changes in precipitation in the Monsoon, CSACZ and SESA regions during spring and summer, warm season circulation features associated with moisture transport into the regions are investigated. These include changes in the SAAC whose western flank forms part of the convergence in the SACZ, and SALLJ which transports moisture from the Amazon Basin to SESA.

### *3.3.1 Sea level pressure*

The poleward expansion of the summer hemisphere subtropical anticyclones is a robust circulation response seen in the climate models globally, e.g., Vecchi and Soden (2007) and Christensen et al. (2007). The sea level pressure (SLP) changes in the A2 scenario simulations compared to the 20C simulations for the South Atlantic are consistent with this expectation. Figure 7 shows the model ensemble seasonal mean SLP differences (A2-20C). In all seasons SLP increases in a zonal region between 30°S–55°S. In winter, this represents the poleward shift of the South Atlantic storm track (Yin 2005). The contours in the figure indicate the 1020 hPa isoline for the 20C (black solid) and for the A2 (black dashed) integrations. The models simulate a poleward expansion of the SAAC in the 21st century. Together with these changes, a small but consistent SLP decrease over the center of the continent is also simulated. The multi-model mean SLP change is representative of all models, with the exception of HadCM3 which simulates almost no change in the SLP pattern over the South Atlantic Ocean throughout the year.

Figure 8 shows the annual evolution of the latitude of the maximum SLP in the South Atlantic Ocean, as well as the value of this maximum (Fig. 8a, b) for NNRP (black) and the multi-model statistics (box plots). These two parameters are used as indicators of the temporal evolution of the SAAC and show its location is furthest south during late summer (Feb–Apr: 32°S) and centered at 28°S during winter (May–

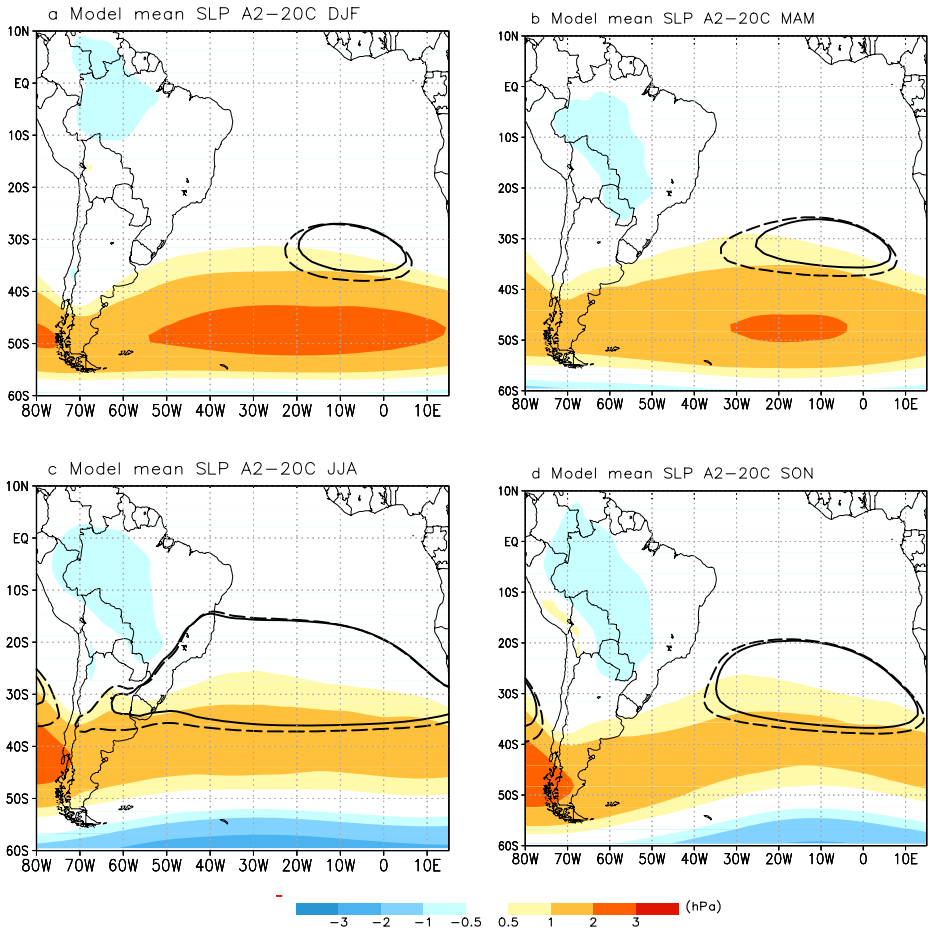


**Fig. 7** Multi-model mean SLP A2-20C difference (*colors*) for DJF (**a**) MAM (**b**) JJA (**c**) and SON (**d**). 1020 hPa isobar for 20C (*solid black*) and for A2 (*dashed black*)

Sep). The NNRP shows that SLP in the SAAC has highest values in winter (July: 1025 hPa) and lowest in summer (March: 1020 hPa). The models capture the seasonal evolution of the SAAC in its latitudinal position though with a southern bias seen in the median during summer. The ensemble median maximum SLP is overestimated by about 1 hPa much of the year and models exhibit more spread in this measure.

There is agreement among the models that the position of the maximum SLP will be located further south (Fig. 8c, about 1 degree) during summer as seen in the median change in the A2 scenario. The difference in the means are statistically significant at the 90% level in every month except Oct. The southward displacement is accompanied by a small increase (≈0.5–1 hPa) through much the year (Fig. 8d). There is less agreement among the models regarding the increase in intensity yet positive differences in the means are significant Jan–Apr (not shown). The poleward shift, however, in the SAAC is well documented (Vecchi and Soden 2007; Solomon

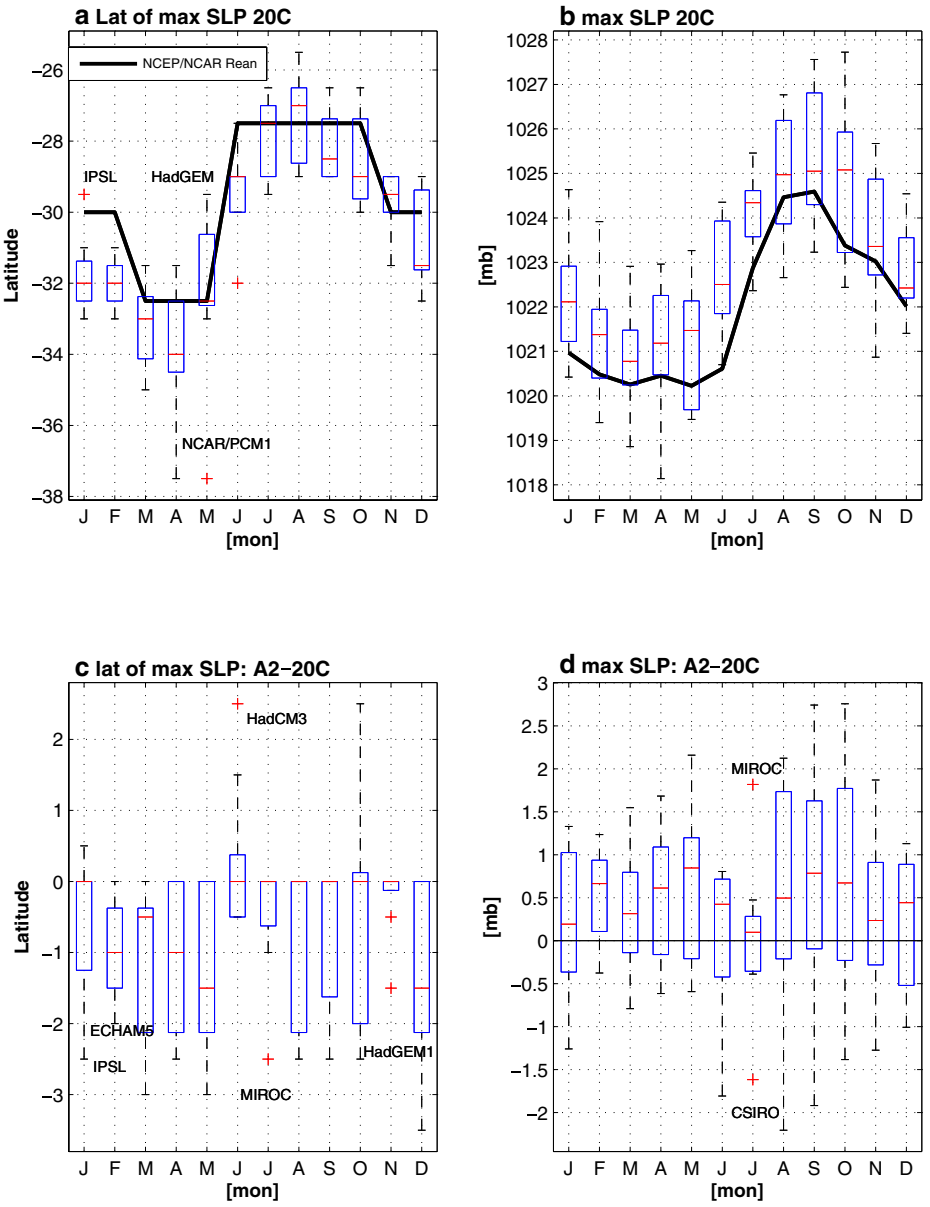


**Fig. 8** Monthly mean position of Sea Level Pressure maximum over the Atlantic ocean, with multi-model statistics and reanalysis (*black*) (**a**). Value of maximum SLP (**b**). Multi-model A2-20C differences in position of maximum SLP (**c**), and differences in maximum SLP (**d**)

and Qin 2007) and is important because it displaces the region of the SACZ poleward, as we have seen in Fig. 6. Therefore, it would appear that the SACZ is shifting southward with the large-scale circulation, rather than as a response to a preferred mode of the SACZ dipole.

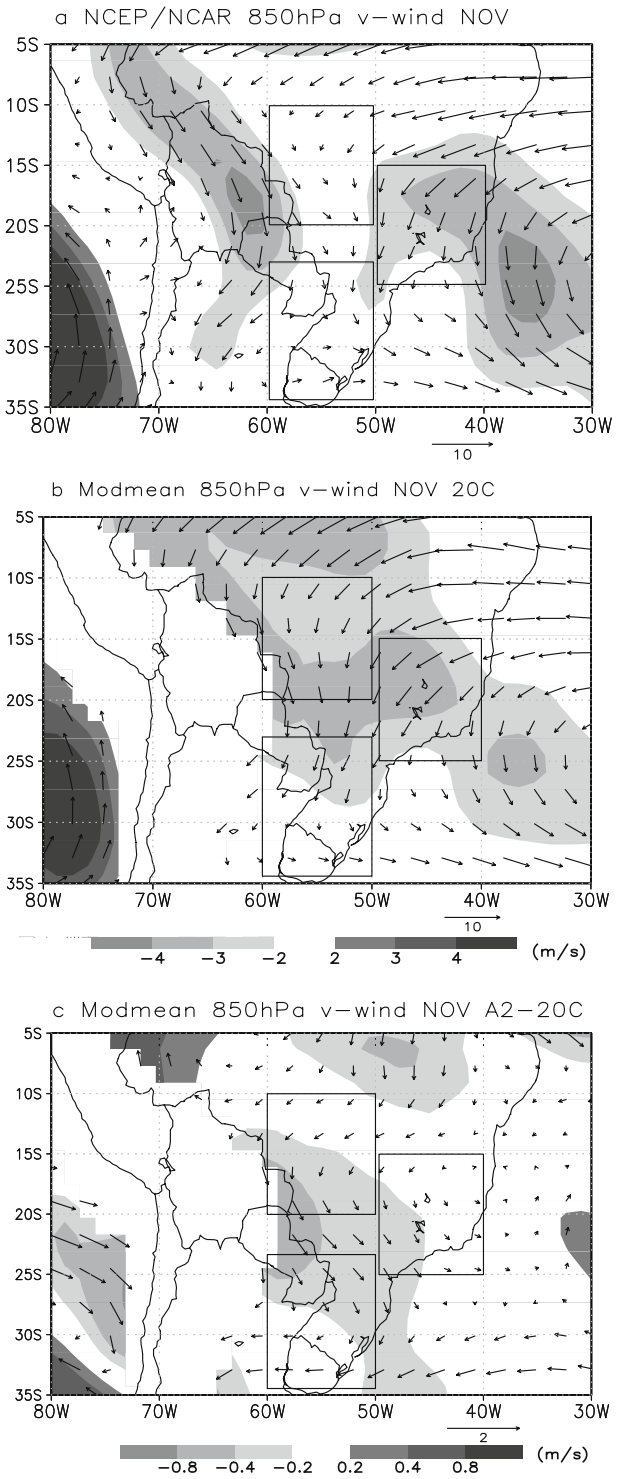


**Fig. 9** November mean meridional wind (*shaded*) and total wind (*vectors*) at 850 hPa for Reanalysis (**a**) and for the model ensemble mean 20C (**b**), and A2-20C (**c**)

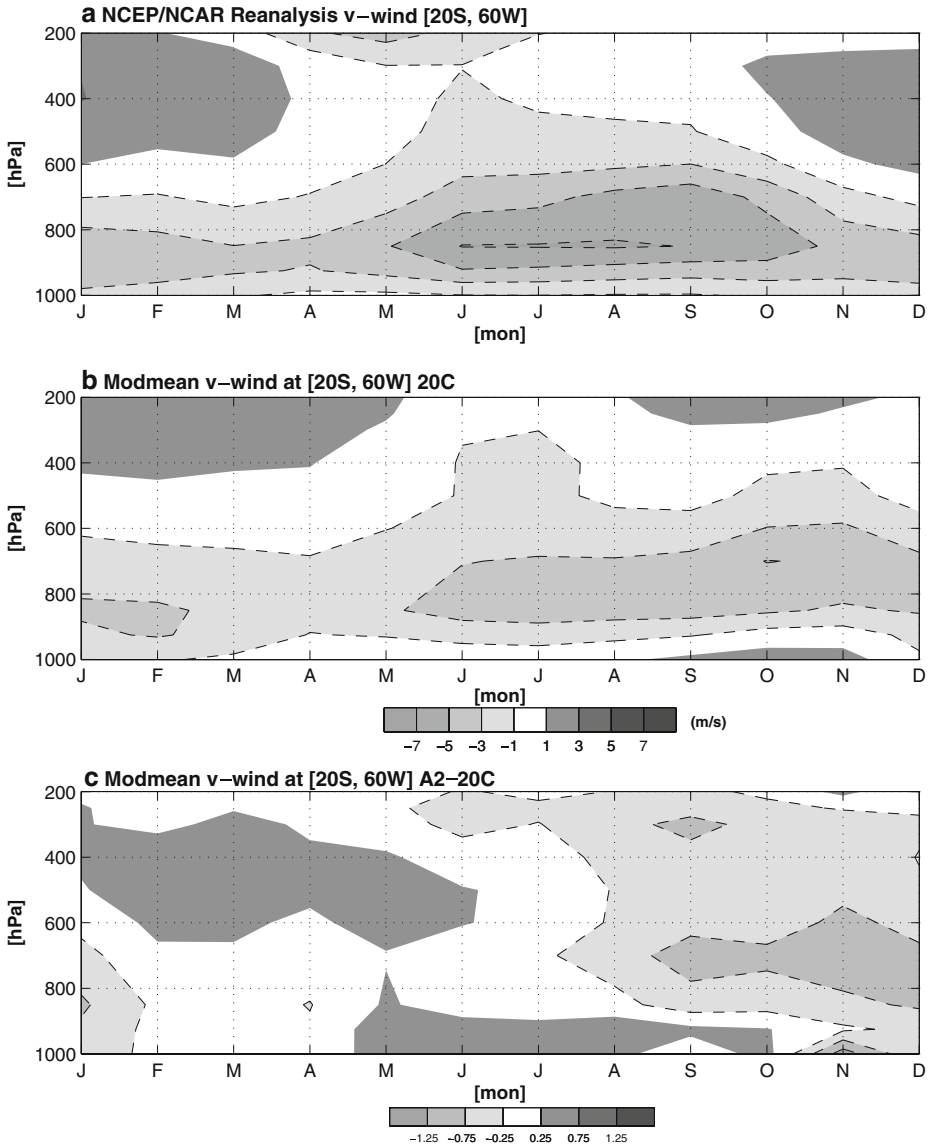


**Fig. 10** Pressure versus time cross section of meridional wind at 20°S and 60°W for Reanalysis (**a**), the multi-model average for 20C (**b**), and A2-20C (**c**)

### *3.3.2 SALLJ*

Changes in the large scale SLP and sub-tropical anticyclones are also likely to affect the low level northerly flow associated with the SALLJ (see previous discussion in Section 1 for the usage of SALLJ), which transports moisture from the wet Amazon basin towards the extratropics into the SESA region. Inspection of the

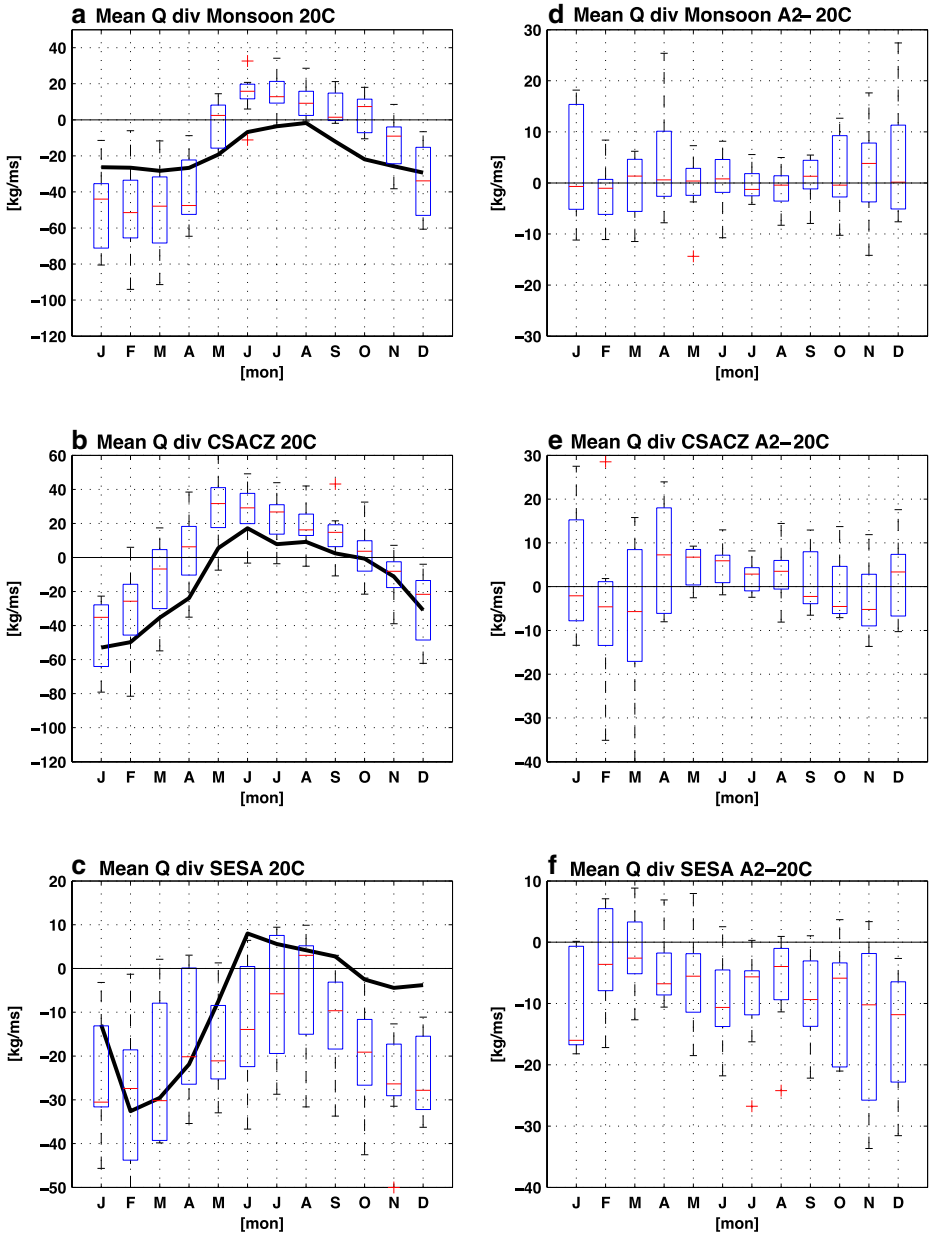


**Fig. 11** Monthly mean vertically integrated moisture flux divergence (Qdiv, kg/ms) from NNRP (*black*) and the multi-model statistics (*box plots*) for the **a**, **d** Monsoon, **b**, **e** CSACZ and **c**, **f** SESA regions, for 20C (**a**, **b**, **c**) and A2-20C differences (**d**, **e**, **f**). Negative (positive) values indicate convergence (divergence) of Q

low-level circulation in the models indicates that HadGEM1 and ECHAM5, which employ higher horizontal resolutions, reproduce this feature comparably with the NNRP (not shown). Figure 9a, b shows meridional winds (shading) at 850 hPa during

November from NNRP and for the multi-model ensemble. The model ensemble mean represents a broader than observed region of northerly flow, with higher wind speeds along the Andes. Note, the models also simulate the northerly flow associated with the SAAC. The low level circulation changes are given in Fig. 9c and show a strengthening of the northerly flow associated with SALLJ. This result is consistent with an increase in the number of SALLJ events reported by Vera et al. (2006b) (their Figure 12a).

Figure 10a, b, c shows the annual evolution of the mean meridional wind profile near the center of the maximum low level flow (20°S and 60°W) in the NNRP, the multi-model ensemble and A2-20C difference. The NNRP shows a low level northerly flow present through the year, with a maximum during late winter. The model ensemble mean low level northerly flow is weaker than that seen in NNRP and shows an increase in wind speed during spring and early summer (Sep–Jan). The intensification of the low level northerly flow is consistent with an increased pressure gradient resulting from the decreased SLP over the interior of the continent and the expansion of the SAAC (see Fig. 7). The projected increase in low level northerly flow associated with SALLJ may be related to the increased precipitation in SESA as a vehicle for enhanced moisture transport, which is examined next.

### 3.4 Changes in moisture transport

To evaluate how the above described precipitation and circulation changes relate to the broader moisture transport changes in the region, we have computed the vertically integrated moisture transport (Q) using the following expression:

$$Q = \frac{1}{g} \int qV dp \tag{1}$$

where g is the acceleration of gravity, q the specific humidity and V the horizontal wind. For the present day simulation, the model-simulated Q has been compared with the one computed from the NCEP/NCAR Reanalysis.

Figure 11 shows the regional mean evolution of the divergence of Q (hereafter, Qdiv) for the NNRP estimate (black) and the mulit-model ensemble statistics (box plots). Negative (positive) values indicate convergence (divergence).

Figure 11a shows that the phase of the annual cycle of Qdiv in the Monsoon region is well simulated by the ensemble median, but most models overestimate the amplitude of the annual cycle (i.e., more divergence in winter and more convergence in summer). There is also greater spread among the models during summer. The CSACZ region exhibits a larger annual cycle than the Monsoon region and here the model tends to overestimate divergence except in spring. In SESA (Fig. 11b)

**Fig. 12** Vertically integrated moisture flux (*vectors*, kg/ms) and its divergence (*shading*) for SON (**a**, **c**, **e**) and DJF (**b**, **d**, **f**) from NNRP (**a**, **b**), the multi-model mean for 20C (**c**, **d**) and A2-20C difference (**e**, **f**). *Shading positive* indicates divergence, *negative* convergence. *Boxes* represent Monsoon, CSACZ and SESA regions ▶

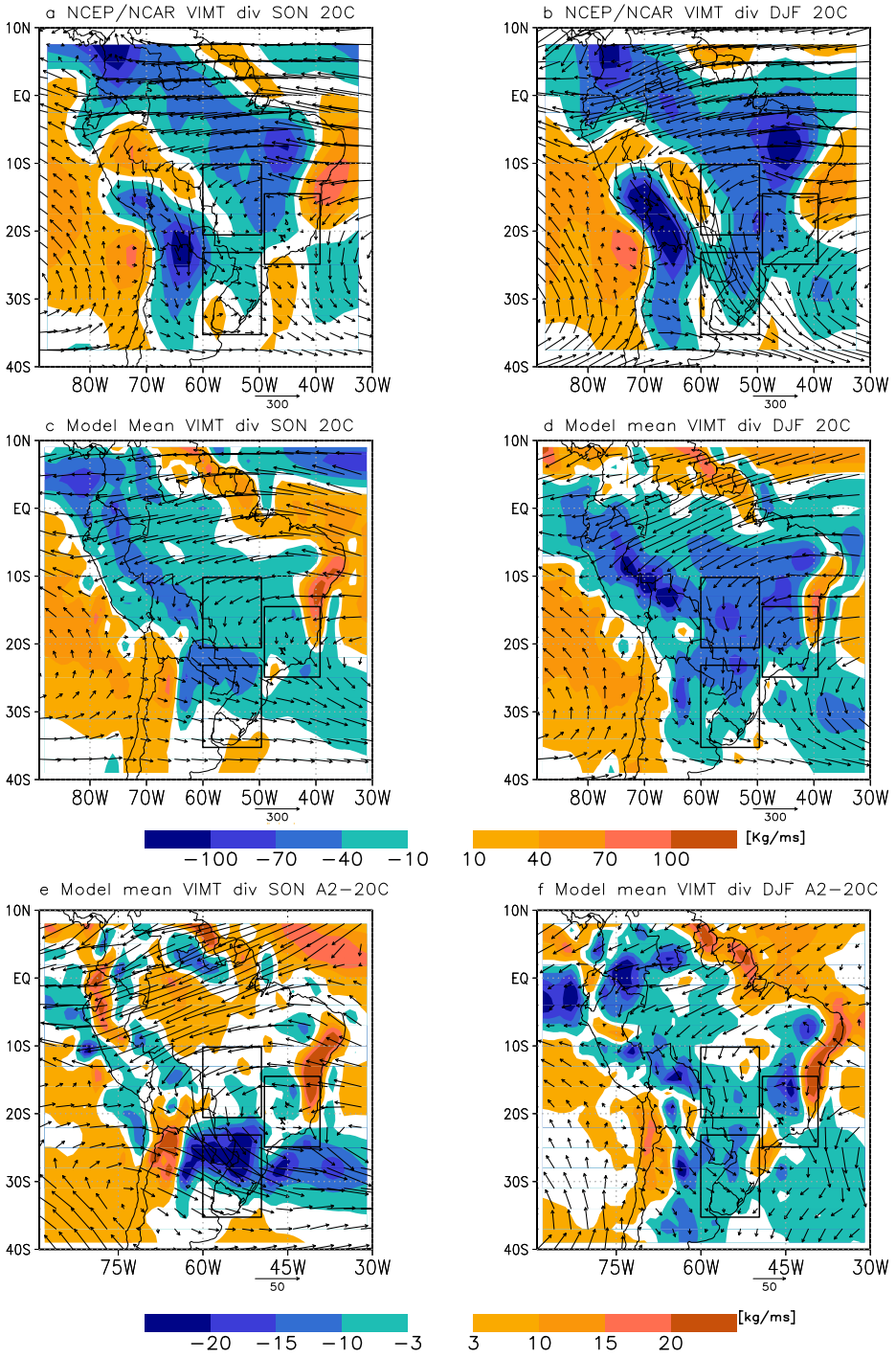
a NCEP/NCAR VIMT div SON 20C
b NCEP/NCAR VIMT div DJF 20C
c Model Mean VIMT div SON 20C
d Model mean VIMT div DJF 20C
e Model mean VIMT div SON A2−20C
f Model mean VIMT div DJF A2−20C
10N
EQ
10S
20S
30S
40S
80W 70W 60W 50W 40W 30W
75W 60W 45W 30W
300
50
−100 −70 −40 −10
10 40 70 100
[Kg/ms]
−20 −15 −10 −3
3 10 15 20
[kg/ms]

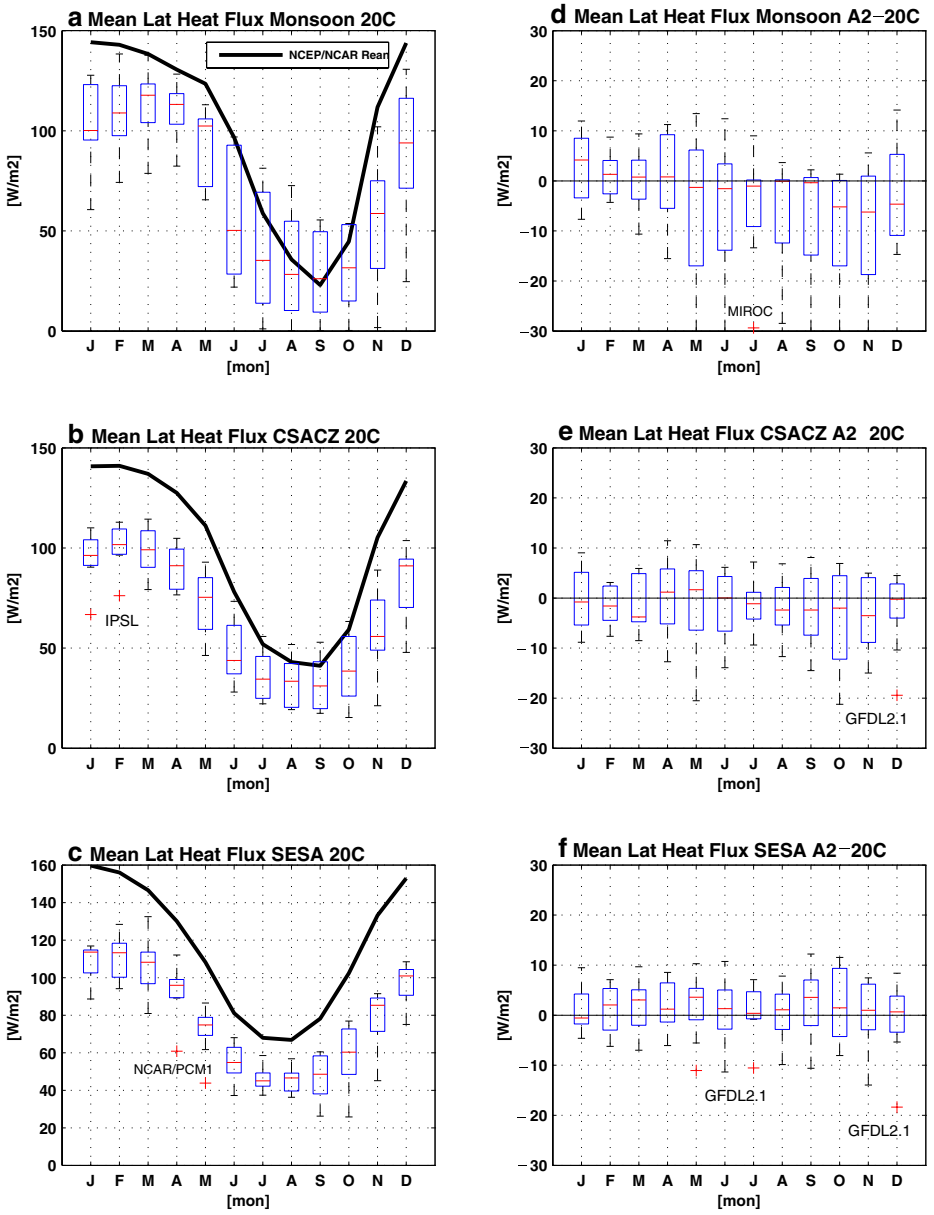


**Fig. 13** Monthly latent heat flux ($W/m^2$) from NNRP (*black*) and the multi-model statistics (*box plots*) for Monsoon (**a**, **d**), CSACZ (**b**, **e**) and SESA (**c**, **f**) regions, for 20C (**a**, **b**, **c**) and A2-20C differences (**d**, **e**, **f**)

the spread among the models is large, as is the case with the precipitation, but the median convergence is captured by the model ensemble which simulates convergence throughout the year.

The differences in the moisture divergence for the A2 scenario with respect to the 20C simulations are shown in Fig. 11d, e, f. In the Monsoon region, the multi-model ensemble indicates generally unchanged moisture convergence, with a hint towards increased divergence during spring, that are significant (Mar–Dec). The CSACZ region shows a slightly increased divergence during the dry season and slightly increased convergence during the wet season, amplifying the annual cycle. These are also significant except in Feb–Mar. In SESA the multi-model ensemble suggests increased moisture convergence throughout the year, with the largest increases during spring and early summer. Changes are significant for all months except Feb.

In order to qualitatively asses the origin of moisture, we examined the spatial patterns of vertically integrated moisture flux (vectors) and its divergences (shading) in Fig. 12, where positive values indicate divergence and negative values convergence. Figure 12a, b show the NNRP estimates for spring (SON) and summer (DJF), respectively. During summer, the models capture well the convergence of moisture in all three regions seen in NNRP, with easterly moisture flux from the subtropical Atlantic into both CSACZ and Monsoon regions, and northerly flux into SESA from the Monsoon region (Fig. 12c, d). In the A2 projections, while the net convergence appears unchanged during spring in the Monsoon and CSACZ regions, there is a substantial increase in SESA convergence during this season, with much of the moisture flux from the north and northwest. During the main rainy season, all three regions show increased moisture convergence, with the Monsoon and SESA regions seeing moisture flux from the north and northwest.

This increased moisture flux from the northwest in SESA is consistent with an expanded SAAC that is found in the differences of the A2 and 20C runs (see Fig. 7). The expanded and poleward displaced SAAC creates an increased east-west pressure gradient which appears to increase the strength of the low level northerly flow and its associated moisture transport from tropical South America to subtropical South America (Virji 1981; Paegle 1998). As shown in Fig. 10, the models indicate a stronger northerly low level flow in the A2 scenarios compared to the 20C simulations. Given the quality and spread of the model results, these linkages are tentative at best, and need to be further explored.

In addition to moisture flux divergence, and important source of moisture to the atmosphere is evapotranspiration, which is related to latent heat flux by the latent heat of vaporization. We examine latent heat flux ($W/m^2$) in Fig. 13, which shows NNRP (black) and multi- model statistics (box plots). The Reanalysis latent heat flux indicates that the annual cycle has a smaller amplitude in SESA than in the Monsoon and CSACZ regions, as expected. The minimum latent heat flux occurs at the end of the dry season (Sep) in the Monsoon region and during the coldest months in SESA (Jul–Aug). The models reproduce the phase of the annual cycle in the regions, although they underestimate the latent heat flux during the warm season in the Monsoon and CSACZ regions and through out the year in SESA. A2-20C changes in latent heat flux (Fig. 13c, d) indicate a small decrease in median latent heat flux in spring (OND) in the Monsoon and CSACZ regions, which coincides with the period of largest warming in the region (see Fig. 4). The statistical significance is achieved for negative differences between the means from Apr–Oct in the Monsoon region and Jun–Nov in CSACZ. This result further supports the possibility that the dry season in the Monsoon region is both intensified and lengthened to weaken the onset of rains in the A2 scenario (Fig. 5c). In SESA a slight increase in ensemble

median latent heat flux through much of the year with significant positive differences between the means in Dec, Feb and Apr–Sep.

## 4 Discussion and conclusions

In this research, nine models from the Coupled Model Intercomparison Project version 3 dataset are employed to examine projected changes in the SAMS annual cycle by comparing the 20th Century and SRES A2 scenarios. The analysis has focused on the Monsoon, CSACZ and SESA regions which comprise important population and economic centers for the continent and have related variability in present day climate. The following hypotheses are examined: (1) the climate responses in the Southeast and Monsoon regions are related by regional circulation and moisture transport changes which, in turn, must be consistent with robust large-scale changes in the climate system, and (2) whether or not these climate responses are consistent with an increased threshold for convection in a warmer world, as indicated by changes in the timing of warm season rains.

The present analysis reaffirms that the Southeast region is likely to experience increased precipitation through the warm season, as reported by Vera et al. (2006b). While the Monsoon and CSACZ region results show larger spread among the models, the multi-model median suggests drying during spring (Sep–Nov), with statistically significant changes in the mean. These continental precipitation changes are accompanied by a statistically significant southward shift of the maximum precipitation in the SACZ. Changes in circulation include a poleward displaced SAAC, which is well documented in the literature (Vecchi and Soden 2007; Christensen et al. 2007). Southward moisture transport also appears to be enhanced, associated with a strengthened northerly low level flow east of the Andes during spring. These changes are consistent with recent observed changes in the SALLJ and SESA precipitation (Vera et al. 2006b; Liebmann et al. 2004). Similar changes are also seen in 21st century projections of the North American Great Plains low-level jet and related to an expansion of the North Atlantic Anti-Cyclone (Cook et al. 2008; Rauscher et al. 2008).

Liebmann et al. (2004), however, suggest this increase in precipitation is associated, though not causally, with weakened winds in the western circulation of the SAAC and increased SST in the sub-tropical South Atlantic near the coast of SESA. While the SAAC intensifies and expands poleward, it also reduces in amplitude toward the equator in the process of shifting towards higher latitudes. The Liebmann et al. (2004) study period was 1976–1999, which they acknowledged was a short period for a robust analysis of mechanisms, and they did speculate that a southward shift in the SACZ was in progress.

Moisture flux divergence calculations indicate unchanged divergence in the Monsoon region during spring and significant increased convergence in the Southeast throughout the warm season. The circulation and moisture transport changes suggest the increased precipitation in the Southeast during spring may be related to changes in the SALLJ and SAAC, which both enhance moisture transport to the Southeast. The onset of the SAMS in the core monsoon region appears to be weakened in the A2 scenario. The changes in the timing of the rainy season may be attributable to robust changes in circulation in the region and globally (Vecchi and Soden 2007),

and are consistent with an increased threshold for convection in the warmer, more humid and stable climate of the 21st century (Neelin et al. 2003; Lintner and Neelin 2006).

The results here suggest a statistically significant possibility that the Monsoon and CSACZ regions will experience a warmer and drier spring. The projected temperature increases would likely lead to increased surface latent heat flux which would require more precipitation simply to maintain present-day moisture conditions. If precipitation were to decrease in the early rainy season, as indicated by the model median, the drying tendency would be further exacerbated, raising implications for water resources management in these population and agricultural centers of the continent.

This study has examined the annual cycle projected multi-model statistics with an emphasis on warm season precipitation. There is substantial variability and disagreement among the models, and the results presented suggest relatively small changes compared with the multi-model variance. Nevertheless, the statistically significant changes and the consistency of these results with expected robust large scale changes provides a measure of confidence in otherwise tentative results. Further testing of these relationships will be required, particularly because these regions of South America experience important modes of variability on intra-seasonal, interannual, and inter-decadal timescales, to understand projected changes in the South American Monsoon.

**Acknowledgements** The authors thank Carolina Vera and Claudio Piani for very helpful discussions and two anonymous reviewers for constructive comments which have lead to significant improvements in the presentation of this research. We thank Dr. Xunqiang Bi for downloading and processing some of the data used in this analysis, and Jeanne Thibeault for assistance with statistical analysis. M. Rojas thanks project ACT19. We acknowledge the international modeling groups for providing their data for analysis, the Program for Climate Model Diagnosis and Intercomparison (PCMDI) for collecting and archiving the model data, the JSC/CLIVAR Working Group on Coupled Modelling (WGCM) and their Coupled Model Intercomparison Project (CMIP) and Climate Simulation Panel for organizing the model data analysis activity, and the IPCC WG1 TSU for technical support. The IPCC Data Archive at Lawrence Livermore National Laboratory is supported by the Office of Science, U.S. Department of Energy.

## References

Allen MR, Stott PA, Mitchell JFB, Schnur R, Delworth TL (2000) Quantifying the uncertainty in forecasts of anthropogenic climate change. Nature 407:617–620. doi:10.1038/35036559

Berbery EH, Barros VR (2002) The hydrologic cycle of the La Plata basin in South America. J Hydrometeorol 3:630–645

Carvalho LMV, Jones C, Liebmann B (2002) Extreme precipitation in southeastern South America and large scale convective patterns in the South Atlantic convergence zone. J Climate 15:2377–2394

Carvalho LMV, Jones C, Liebmann B (2004) The South Atlantic Convergence Zone: intensity, form, persistence, and relationships with intraseasonal to interannual activity and extreme rainfall. J Climate 17:88–108

Christensen JH, Hewitson B, Busuioc A, Chen A, Gao X, Held I, Jones R, Kolli RK, Kwon WT, Laprise R, Rueda VM, Mearns L, Menéndez CG, Räisänen J, Rinke A, Sarr A, Whetton P (2007) Regional climate projections. In: Solomon S, Qin D, Manning M, Chen Z, Marquis M, Averyt K, Tignor M, Miller H (eds) Climate change 2007: the physical science basis. Contribution of working group I to the fourth assessment report of the intergovernmental panel on climate change, chap. 11. Cambridge University Press, New York, pp 235–336

Cook KH, Vizy EK, Launer ZS, Patricola CM (2008) Springtime intensification of the great plains low-level jet and midwest precipitation in GCM simulations of the 21st century. J Climate. doi:10.1175/2008JCLI2355.1

Diaz A, Aceituno P (2003) Atmospheric circulation anomalies during episodes of enhanced and reduced convective cloudiness over Uruguay. J Climate 16:3171–3185

Gan MA, Kousky VE, Ropelewski CF (2004) The South American Monsoon circulation and its relationship to rainfall over West-Central Brazil. J Climate 17:47–66

Gan MA, Rao VB, Moscati CL (2006) South American Monsoon indices. Atmos Sci Lett 6:219–223. doi:10.1002/asl.119

Giorgi F, Bi X (2005) Updated regional precipitation and temperature changes for the 21st century from ensembles of AOGCM simulations. Geophys Res Lett 33:l21715

Held IM, Soden BJ (2006) Robust responses of the hydrological cycle to global warming. J Climate 19:5686–5699

Herdies DL, da Silva A, Silva Dias MAF, Nieto Ferreira R (2002) Moisture budget of the bimodal pattern of the summer circulation over South America. J Geophys Res 107(D20):8075. doi:10.1029/2001JD000997

Kalnay E, Kanamitsu M, Kistler R, Collins W, Deaven D, Gandin L, Iredell M, Saha S, White G, Woollen J, Zhu Y, Leetmaa A, Reynolds B, Chelliah M, Ebisuzaki W, Higgins W, Janowiak J, Mo KC, Ropelewski C, Wang J, Jenne R, Joseph D (1996) The NCEP/NCAR 40-year reanalysis project. Bull Am Meteorol Soc 77:437–472

Kharin VV, Zwiers FW, Zhang X, Hegerl GC (2007) Changes in temperature and precipitation extremes in the IPCC ensemble of global coupled model simulations. J Climate 20:1419–1444

Kodama YM (1992) Large-scale common features of subtropical precipitation zones (the Baiu frontal zone, the SPCZ, and the SACZ). Part I: characteristics of the subtropical frontal zones. J Meteorol Soc Jpn 70:813–836

Kodama YM (1993) Large-scale common features of subtropical precipitation zones (the Baiu frontal zone, the SPCZ, and the SACZ). Part II: conditions of the circulation for generating the STCZs. J Meteorol Soc Jpn 71:581–610

Kousky VE, Kagano MT, Cavalcanti IFA (1984) A review of the Southern Oscillation: oceanic-atmospheric circulation changes and related rainfall anomalies. Tellus Series A 36:490

Li W, Fu R, Dickinson RE (2006) Rainfall and its seasonality over the Amazon in the 21st century as assessed by the coupled models for the IPCC AR4. J Geophys Res 111:D02111. doi:10.1029/2005JD006355

Liebmann B, Vera CS, Carvalho LMV, Camilloni IA, Hoerling MP, Allured D, Barros VR, Báez J, Bidegain M (2004) An observed trend in Central South American precipitation. J Climate 17:4357–4367

Lintner BR, Neelin JD (2006) A prototype for convective margin shifts. Geophys Res Lett 34. doi:10.1029/2006GL027305

Marengo J (1992) Interannual variability of surface climate in the Amazon basin. Int J Climatol 12:853–863

Marengo JA, Douglas M, Silva Dias P (2002) The South American low level jet East of the Andes during LBA-TRMM and WET AMC campaign of January–April 1999. J Geophys Res 107(47):1–11

Marengo JA, Soares WR, Saulo C, Nicolini M (2004) Climatology of the low level jet East of the Andes as derived from NCEP-NCAR reanalyses: characteristics of temporal variability. J Climate 17(12):2261–2280

Meehl GA, Covey C, Delworth T, Mojib L, McAvaney B, Mitchell JFB, Stouffer RJ, Taylor KE (2007) The WCRP CMIP3 multimodel dataset: a new era in climate change research. Bull Am Meteorol Soc 88:1383–1394

Neelin JD, Chou C, Su H (2003) Tropical drought regions in global warming and El Niño teleconnections. Geophys Res Lett 30(24):2275. doi:10.1029/2003GL018625

Nogués-Paegle J, Mo KC (1997) Alternating wet and dry conditions over South America during summer. Mon Weather Rev 125:279–291

Paegle J (1998) A comparative review of South American low-level jets. Meteorologica 23:73–81

Rauscher SA, Giorgi F, Diffenbaugh NS, Seth A (2008) Extension and intesification of the Meso-American mid-summer drought in the twenty-first century. Clim Dyn 31:551–571. doi:10.1007/s00382-007-0359-1

Ropelewski CF, Halpert MS (1987) Global and regional scale precipitation patterns associated with the El Niño Southern Oscillation. Mon Weather Rev 115:1606–1626

Solomon S, Qin D (2007) Climate change 2007: the physical science basis. In: Working group I report to the fourth assessment of the Intergovernmental Panel on Climate Change (IPCC). Cambridge University Press, Cambridge

Vecchi GA, Soden BJ (2007) Global warming and the weakening of the tropical circulation. J Climate 20:4316–4340

Vera C, Baez J, Douglas M, Emmanuel CB, Marengo J, Meitin J, Nicolini M, Nogues-Paegle J, Paegle J, Penalba O, Salio P, Saulo C, Silva Dias MA, Silva Dias P, Zipser E (2006a) The South American low-level jet experiment. Bull Am Meteorol Soc 87:63–77

Vera C, Higgins W, Amador J, Ambrizzi T, Garreaud R, Gochis D, Gutzler D, Lettenmaier D, Marengo J, Nogues-Paegle J, Silva Dias P, Zhang C (2006b) Toward a unified view of the American monsoon systems. J Climate 19:4977–5000

Vera C, Silvestri G, Liebmann B, Gonzalez P (2006c) Climate change scenarios for seasonal precipitation in South America from IPCC-AR4 models. Geophys Res Lett 33. doi:10.1029/2006GL025759

Virji H (1981) A preliminary study of summertime tropospheric circulation patterns over South America estimated from cloud winds. Mon Weather Rev 109:599–610

Wilks DS (2005) Statistical methods in the atmospheric sciences, vol 91, 2nd edn. Academic, London

Xie P, Arkin P (1996) Analysis of global monthly precipitation using gauge observation, satellite estimates and numerical model predictions. J Climate 9:840–858

Yin JH (2005) A consistent poleward shift of the storm tracks in simulations of 21st century climate. Geophys Res Lett 32:L18701. doi:10.1029/2005GL023684

Zhou J, Lau KM (1998) Does a monsoon climate exist over South America? J Climate 11:1020–1040